Nanosize Cation-Disordered Rocksalt Oxides; Na_2TiO_3-$NaMnO_2$ Binary System

Tokio Kobayashi[a], Wenwen Zhao[b, c], Hongahally Basappa Rajendra[a], Keisuke Yamanaka[d], Toshiaki Ohta[d], and Naoaki Yabuuchi[a, c]*

[a]Department of Chemistry and Life Science, Yokohama National University, 79-5 Tokiwadai, Hodogaya-ku, Yokohama, Kanagawa 240-8501, Japan

[b]Department of Applied Chemistry, Tokyo Denki University, Adachi, Tokyo 120-8551, Japan

[c]Elements Strategy Initiative for Catalysts and Batteries, Kyoto, f1-30 Goryo-Ohara, Nishikyo-ku, Kyoto 615-8245, Japan

[d]SR Center, Ritsumeikan University, 1-1-1 Noji-Higashi, Kusatsu, Shiga 525-8577, Japan

*corresponding author

E-mail: yabuuchi-naoaki-pw@ynu.ac.jp

Abstract

To realize the development of rechargeable sodium batteries, new positive electrode materials without less abundant elements have been explored. Enrichment of sodium contents in host structures is required to increase in theoretical capacity as electrode materials, and therefore Na-excess compounds are systematically examined in a binary system of Na_2TiO_3–$NaMnO_2$. After several trials, it is succeeded in synthesis of Na-excess compounds with a cation disordered rocksalt structure by adapting mechanical milling method. Among the tested electrode materials, $Na_{1.14}Mn_{0.57}Ti_{0.29}O_2$ in this binary system delivers a large reversible capacity of *ca*. 200 mA h g^{-1}, originating from reversible redox reactions of cationic Mn^{3+}/Mn^{4+} and anionic O^{2-}/O^{n-} redox confirmed by X-ray absorption spectroscopy. Holes in oxygen 2p orbitals, which are created by electrochemical oxidation, are energetically stabilized by electron donation from Mn ions. Moreover, reversibility of anionic redox is significantly improved compared with a former study on a binary system of Na_3NbO_3–$NaMnO_2$ tested as model electrode materials.

Abstract; sodium batteries, sodium-excess, manganese, anionic redox, nanosize

The demand on electrochemical energy storage devices is rapidly growing to realize a society with renewable and sustainable energy resources. Although rechargeable Li batteries are possibly used on this purpose, an emerging problem is found in the increasing cost of Li resources associated with the significant growth of the market of electric vehicles equipped with Li batteries. Therefore, research interest on rechargeable Na batteries operable at room temperature has re-emerged as the cost-effective battery system because of abundance of Na in the crust and ocean.[1, 2] Nevertheless, to realize commercialization of Na batteries, the development of positive electrode materials, which have competitive energy density to the Li counterpart, is of primary importance. During the past several years, considerable research efforts have been conducted on Na-containing metal oxides and oxoanionic compounds.[3-10] Furthermore, to design positive electrode materials for Na battery applications, the use of inexpensive and earth-abundant elements is required to reduce materials costs of batteries.[11] As the most abundant transition metal ions, Fe-based materials, such as $NaFeO_2$,[9, 10] $Na_{2/3}Fe_{1/2}Mn_{1/2}O_2$,[8, 12] $Na_2FeP_2O_7$,[3] and $Na_2Fe_2(SO_4)_3$[5] with different crystal structures, have been intensively examined for Na battery applications. Nevertheless, the energy density of these as-prepared electrode materials is not competitive to $LiMn_2O_4$ and $LiFePO_4$ used as cost-effective positive electrode materials for Li batteries. Moreover, emerging chemistry of anionic redox for Li-excess compounds, Li_2MnO_3 and its derivatives, potentially further boosts the energy

density of Li batteries.[13-16] Instead of transition metal ions with d-electrons, oxide ions, as non-cationic species in the structure, donate electrons upon charge compensation during electrochemical Li extraction (oxidation). The development of electrode materials, which simultaneously use classical cationic and anionic redox, is accelerating throughout the world. This approach has been extended to electrode material designs for Na battery applications. It has been demonstrated that oxide ion redox is realized in the Li-containing layered system with Na ions, for instance, P2-type $Na_{5/6}Li_{1/4}Mn_{3/4}O_2$[17] and P3-type $Na_{0.6}Li_{0.2}Mn_{0.8}O_2$.[18] In addition, studies on P2 $Na_{2/3}Mg_{0.28}Mn_{0.72}O_2$ reveals that utilization of anionic redox is activated in the Mg-substituted system.[19, 20] However, these P2 and P3 layered oxides are Na deficient phases, leading to the difficulty to apply these phases to full cells coupled with negative electrode materials without Na ions in structures. Therefore, direct synthesis of Na-excess compounds is preferable for battery applications. The ionic radius of Na is too large when compared with 3d-transition metal ions, leading to crystallization into the non-layered phase. Therefore, publications of Na-excess compounds with the layered structure are limited, and such compounds are mainly found for period 5 and 6 elements with relatively large ionic sizes, for instance, Na_2RuO_3,[21] Na_2SnO_3,[22] and Na_2IrO_3[23].

Recently, our group has reported the synthesis of metastable Na-excess oxides by mechanical milling. $Na_{1.3}Mn_{0.4}Nb_{0.3}O_2$ with a cation-disordered rocksalt-type structure has been

successfully prepared and tested as a model electrode material.[24] Anionic redox is activated in this system associated with a highly ionic character of Nb^{5+} ions. Nevertheless, necessity of Nb, which is an expensive 4d-transition metal ion, possibly hinders its use for practical applications. In this study, this concept is, therefore, extended to Ti ions because Ti^{4+} has a similar character with Nb^{5+}.[16] A binary system of Na_2TiO_3–$NaMnO_2$ is systematically studied as potential high-capacity positive electrode materials with anionic redox. X-ray absorption spectroscopy clearly reveals that high reversible capacity partially originates from anionic redox, coupled with Mn^{3+}/Mn^{4+} cationic redox. From these results, we discuss the possibility of metastable and Na-excess oxides with the rocksalt structure made from only the Earth-abundant elements for cost-effective energy storage applications.

Synthesis of $Na_{1.2}Mn_{0.4}Ti_{0.4}O_2$ ($x = 0.5$ in $x\ Na_2TiO_3 – (1 – x)\ NaMnO_2$) was first carried out by conventional solid-state calcination method. **Supporting Figure S1** shows X-ray diffraction (XRD) patterns of samples directly synthesized from a mixture of Na_2CO_3, TiO_2, and Mn_2O_3 at different heating temperatures. From the XRD patterns, heating of the sample at < 900 ^oC results in the phase segregation into the end members, $NaMnO_2$ and Na_2TiO_3. Schematic illustrations of crystal structures of $NaMnO_2$ and Na_2TiO_3 are shown in **Figure 1a**.

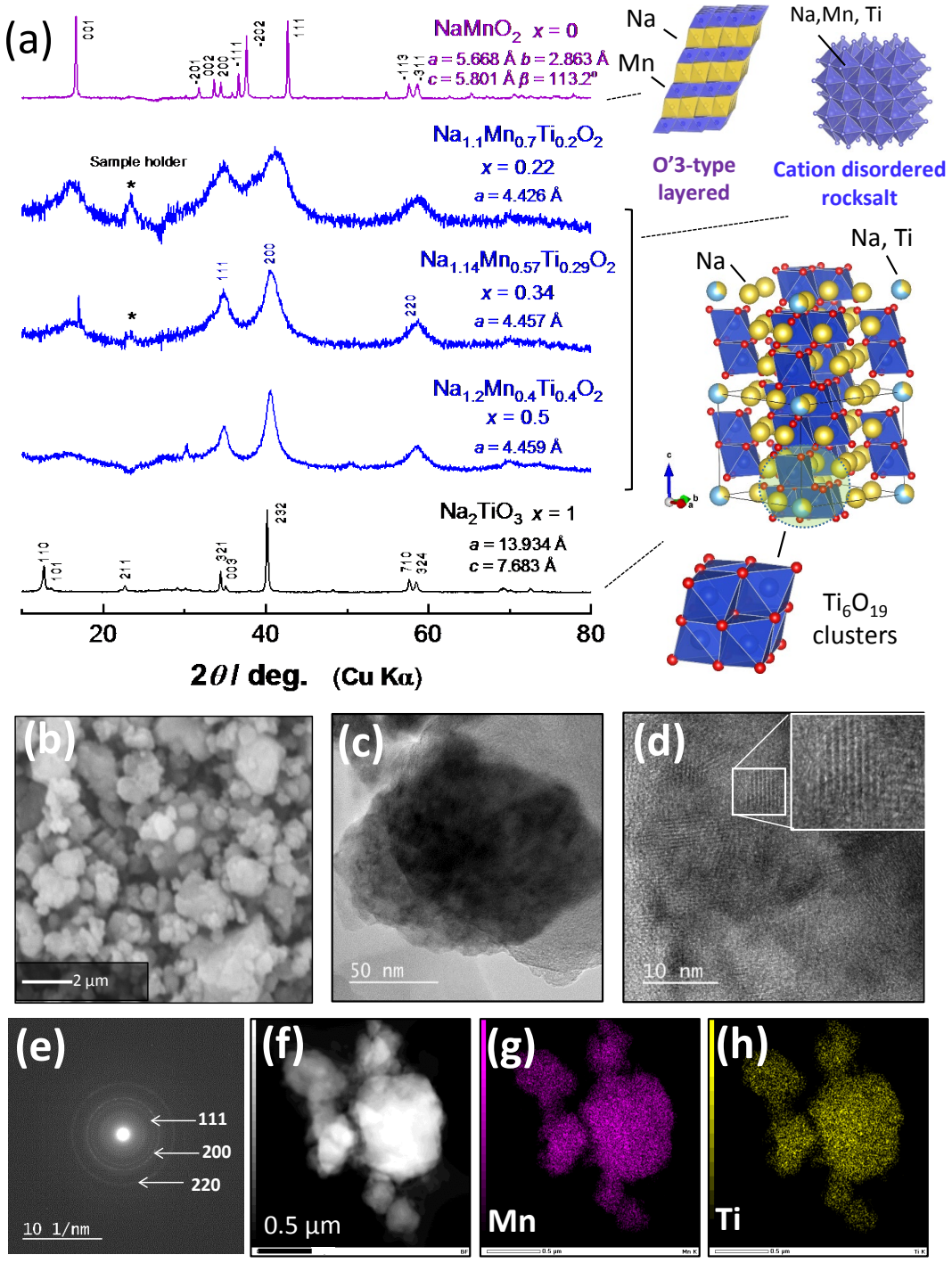

Figure 1. Synthesis of a binary system of x $Na_2TiO_3 - (1 - x)$ $NaMnO_2$ by mechanical milling; (a) XRD patterns of the binary phase, (b) SEM and (c, d) TEM images of $Na_{1.14}Mn_{0.57}Ti_{0.29}O_2$ (x = 0.34), (e) a selected-area electron diffraction pattern of $Na_{1.14}Mn_{0.57}Ti_{0.29}O_2$. (f) A bright-field

image and corresponding STEM-EDS maps of Mn (g) and Ti (h) ions for $Na_{1.14}Mn_{0.57}Ti_{0.29}O_2$. Structural analysis has been conducted by RIETAN-FP.[25] Schematic illustrations of crystal structures were drawn using the VESTA program.[26]

Both end members consist of cubic close-packing of oxide ions, and transition metal and sodium ions are found at octahedral sites. For $NaMnO_2$, MnO_6 and NaO_6 octahedra share edges, forming two-dimensional MnO_2 and NaO_2 layers, respectively, and these two layers are stacked alternately, resulting in the crystallization of a layered structure. Six of TiO_6 octahedra share edges, forming Ti_6O_{19} clusters, and the clusters are surrounded and isolated by Na ions in Na_2TiO_3. Partial anti-site defects between Na and Ti sites are also noted for Na_2TiO_3.[27] This phase is also known as a high-temperature phase among three different polymorphs of Na_2TiO_3.[27] Synthesis of the sample at 1000 ^oC results in crystallization of an unknown phase, but phase segregation of Mn and Ti ions is clearly evidenced by SEM-EDX analysis in **Supporting Figure S2**. Synthesis of this binary system by calcination was unsuccessful, and therefore, mechanical milling approach, which allows to synthesize thermodynamically metastable phases by using mechanical energy, including friction and shear stress, [28-33] was applied. Mechanical impact and friction during milling reduce particle sizes of materials into nanoscale, and many structural defects are induced. These defects possibly disturb long-range cation ordering, leading to the formation of cation-

disordered phases with a high symmetry. Phase transformation is further assisted by shear stress during milling.[33] A detailed synthesis method of samples by mechanical milling is found in **Supporting Information**. **Figure 1a** shows XRD patterns of a binary phase of x Na_2TiO_3 – (1 – x) $NaMnO_2$ with different chemical compositions after mechanical milling at 600 rpm. The XRD patterns of the samples can be indexed into a cation-disordered rocksalt-type structure. Broad diffraction lines indicate the formation of nanosize and a low crystallinity samples, and this trend is generally observed for the samples prepared by mechanical milling. Diffraction patterns of the end members disappear by mechanical milling. Despite a large size gap between Na and Ti/Mn ions, all cations are randomly distributed in the same site of the rocksalt structure, similar to $Na_{1.3}Mn_{0.4}Nb_{0.3}O_2$. A lattice parameter of $Na_{1.14}Mn_{0.57}Ti_{0.29}O_2$ (x = 0.34) is calculated to be 4.457 Å, which is longer than 4.443 Å for $NaMnO_2$ with the rocksalt structure obtained by mechanical milling.[30] This fact also suggests the incorporation of larger Na ions into the rocksalt structure and the formation of Na-excess phases. An average secondary particle size of the sample (x = 0.34) is below 2 μm with a spherical shape as shown in **Figure 1b**. Successful synthesis of the samples is also supported by SEM-EDX as shown in **Supporting Figure S3**, and uniform distributions of Ti and Mn ions are observed in elemental maps. Note that, similar to other materials synthesized by mechanical milling, these phases are metastable phases and therefore segregated into $NaMnO_2$ and Na_2TiO_3 by heating at higher temperatures as shown in

Supporting Figure S4. This result is also consistent with the fact that unsuccessful synthesis of the samples by calcination. To further examine particle morphology and nanostructures of the sample, TEM measurement of $Na_{1.14}Mn_{0.57}Ti_{0.29}O_2$ (x = 0.34) were performed, and the results are shown in **Figure 1c – h**. Nanosized crystalline particles with an average size of 10 nm are observed as shown in **Figure 1d**. An electron diffraction study also reveals a polycrystalline nature of the sample (**Figure 1e**). The presence of diffraction rings is clearly observed, and *d*-spacing of the rings are calculated to be 2.6, 2.2, and 1.6 Å, which correspond to 111, 200, and 220 diffraction rings, respectively. Moreover, a uniform distribution of Na, Mn and Ti ions in nanoscale is clearly evidenced in STEM-EDS images (**Figure 1f, g**, and **h**). From these results, it is concluded that the binary system of Na_2TiO_3–$NaMnO_2$ is successfully crystallized into nanosize oxides with the cation-disordered rocksalt structure by mechanical milling.

Electrode performance of thus obtained samples is tested in Li cells, and charge/discharge curves of the samples are shown in **Figure 2**. For the most Na/Ti rich phase, $Na_{1.2}Mn_{0.4}Ti_{0.4}O_2$ (x = 0.5), a limited reversible capacity of ~150 mA h g^{-1} is obtained, which is slightly larger than a theoretical capacity estimated on the basis of Mn^{3+}/Mn^{4+} redox reaction (106 mA h g^{-1}). This fact suggests that redox reaction of oxide ions is partially activated, but insufficient electronic conductivity and/or low reversibility of anionic redox (oxygen loss is a dominative process) would result in that a limited amount of Na ions is extracted from this phase.

This trend is clearly different from the case of $Li_{1.2}Mn_{0.4}Ti_{0.4}O_2$, which exhibits a high reversible capacity of ~300 mA h g^{-1} with reversible cationic/anionic redox.[16] In contrast, for the samples with lower Na contents, $Na_{1.14}Mn_{0.57}Ti_{0.29}O_2$ and $Na_{1.1}Mn_{0.7}Ti_{0.2}O_2$, drastic enhancement of reversible capacities is observed.

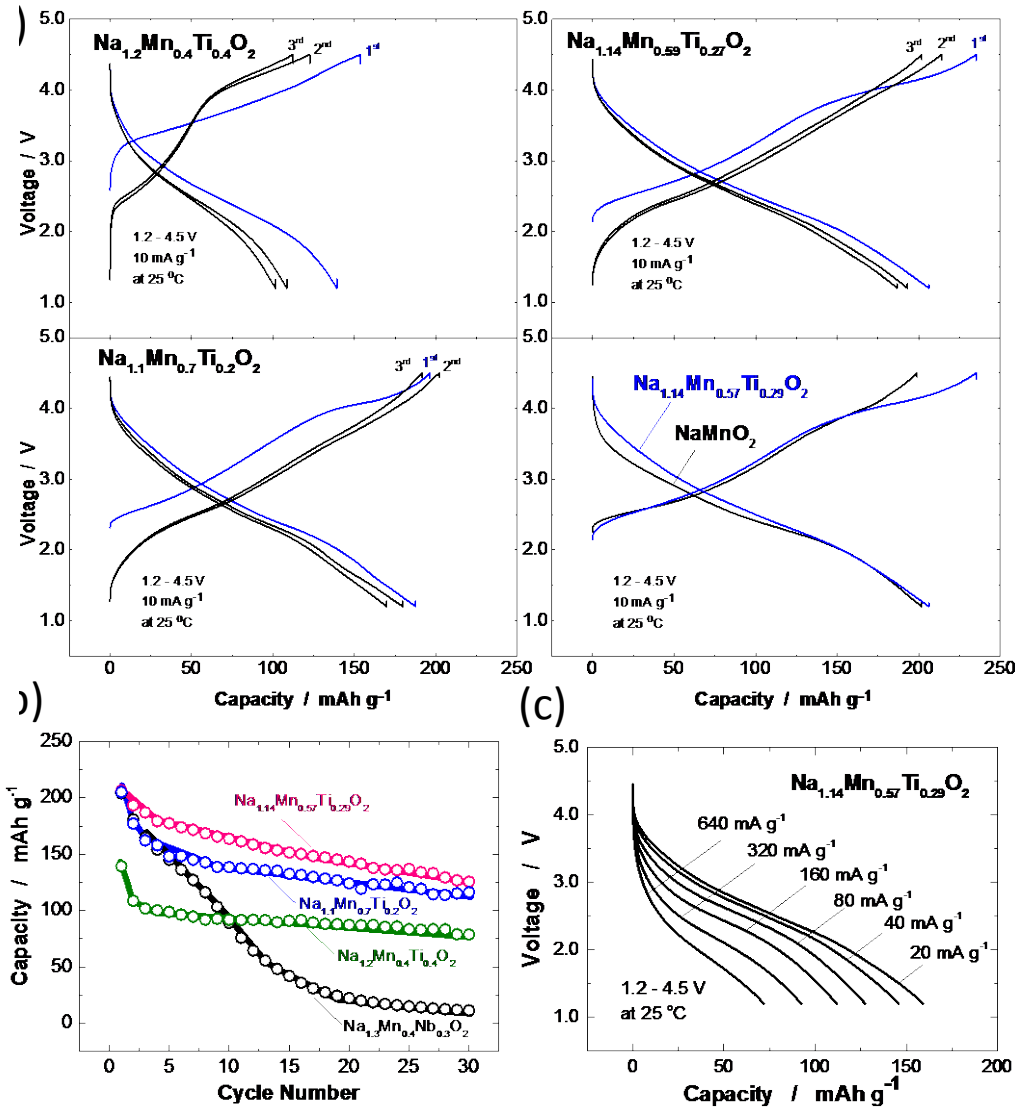

Figure 2. Electrochemical performance of the binary system of x Na_2TiO_3 – (1 – x) $NaMnO_2$;

(a) charge/discharge curves of the samples in Li cells at a rate of 10 mA g^{-1} at room temperature. Capacity retention of the samples is also shown in (b). A result of $Na_{1.3}Mn_{0.4}Nb_{0.3}O_2$ is also shown for comparison.[24] (c) Rate capability of $Na_{1.14}Mn_{0.57}Ti_{0.29}O_2$ in a Na cell. The cells were charged at 10 mA g^{-1} to 4.5 V and held at 4.5 V for 1 h, and then discharged at different rates to 1.2 V. Note that Na_2TiO_3 is electrochemically inactive even after mechanical milling because of an electronically nonconductive oxide.

Observed charge capacities exceed the theoretical capacity estimated from Mn^{3+}/Mn^{4+} cationic redox, indicating the activation of oxygen redox in these samples. Moreover, $Na_{1.14}Mn_{0.57}Ti_{0.29}O_2$ and $Na_{1.1}Mn_{0.7}Ti_{0.2}O_2$ show voltage plateaus at a 4 V region in addition to a slope region in 2.2 – 4.0 V. Such voltage plateaus for initial charge are a characteristic feature of contribution of anionic redox for Li-excess electrode materials.[34] Charge/discharge curves of rocksalt $Na_{1.14}Mn_{0.57}Ti_{0.29}O_2$ and $NaMnO_2$ prepared by mechanical milling are also compared in **Figure 2a**. Nanosize $NaMnO_2$ with the rocksalt structure delivers a reversible capacity of *ca.* 200 mA h g^{-1} with pure cationic redox.[30] In contrast to $NaMnO_2$, presence of the voltage plateau at 4 V is clearly noted for the Na-excess rocksalt oxide, which is also indicative of the use of anionic redox as electrode materials. Additionally, discharge voltage is slightly increased for the Na-excess phase, implying that the utilization of anionic redox is beneficial to enhance the

energy density for battery applications. The capacity retention of the Na_2TiO_3–$NaMnO_2$ binary system is also shown in **Figure 2b**. For comparison, the result of the previously reported $Na_{1.3}Mn_{0.4}Nb_{0.3}O_2$ used as a model material is also plotted.[24] Among the tested samples with different compositions, $Na_{1.14}Mn_{0.57}Ti_{0.29}O_2$ exhibits the best performance in terms of cycle stability with high reversible capacity. Much better capacity retention is realized for the Na_2TiO_3–$NaMnO_2$ binary system, compared with our previous study with Nb ions.[24] It is also expected that further optimization of the chemical compositions would lead to further enhancement of electrode performance. The rate capability of $Na_{1.14}Mn_{0.57}Ti_{0.29}O_2$ is also tested in a Na cell, and a result is shown in **Figure 2c**. The result is competitive with that of nanosize $NaMnO_2$ with the rocksalt structure.[30] The sample delivers large reversible capacity even though it is expected that higher concentration of grain boundaries in particles would be sacrifice facile Na migration as electrode materials. Further understanding is needed to explain good electrode performance for the nanosize oxides with the rocksalt structure.

To further study the reaction mechanisms of $Na_{1.14-y}Mn_{0.57}Ti_{0.29}O_2$ as electrode materials, combination studies of *ex-situ* X-ray diffractometry and X-ray absorption spectroscopy (XAS), including hard and soft X-ray, were carried out. *Ex-situ* synchrotron XRD patterns of the composite electrodes during initial charge are displayed in **Figure 3a**. Lattice parameters of the sample are drastically reduced on charge from 4.426 to 4.19 Å on charge to 4.5 V. In addition,

lowered crystallinity on charge is noted. Observed volume change reaches ~17%, which is significantly larger than that for $Li_{1.2-y}Mn_{0.4}Ti_{0.4}O_2$ sample (~5.6%) as shown in **Supporting Figure S5**. Extraction of large Na ions from the crystal lattice on charge results in the large volume change, and this observation is also consistent with the fact of insufficient capacity retention as electrode materials (**Figure 2b**). Large volume expansion would induce mechanical stress, possibly leading to the formation of crack inside particles and loss of electrical contact on electrochemical cycles.

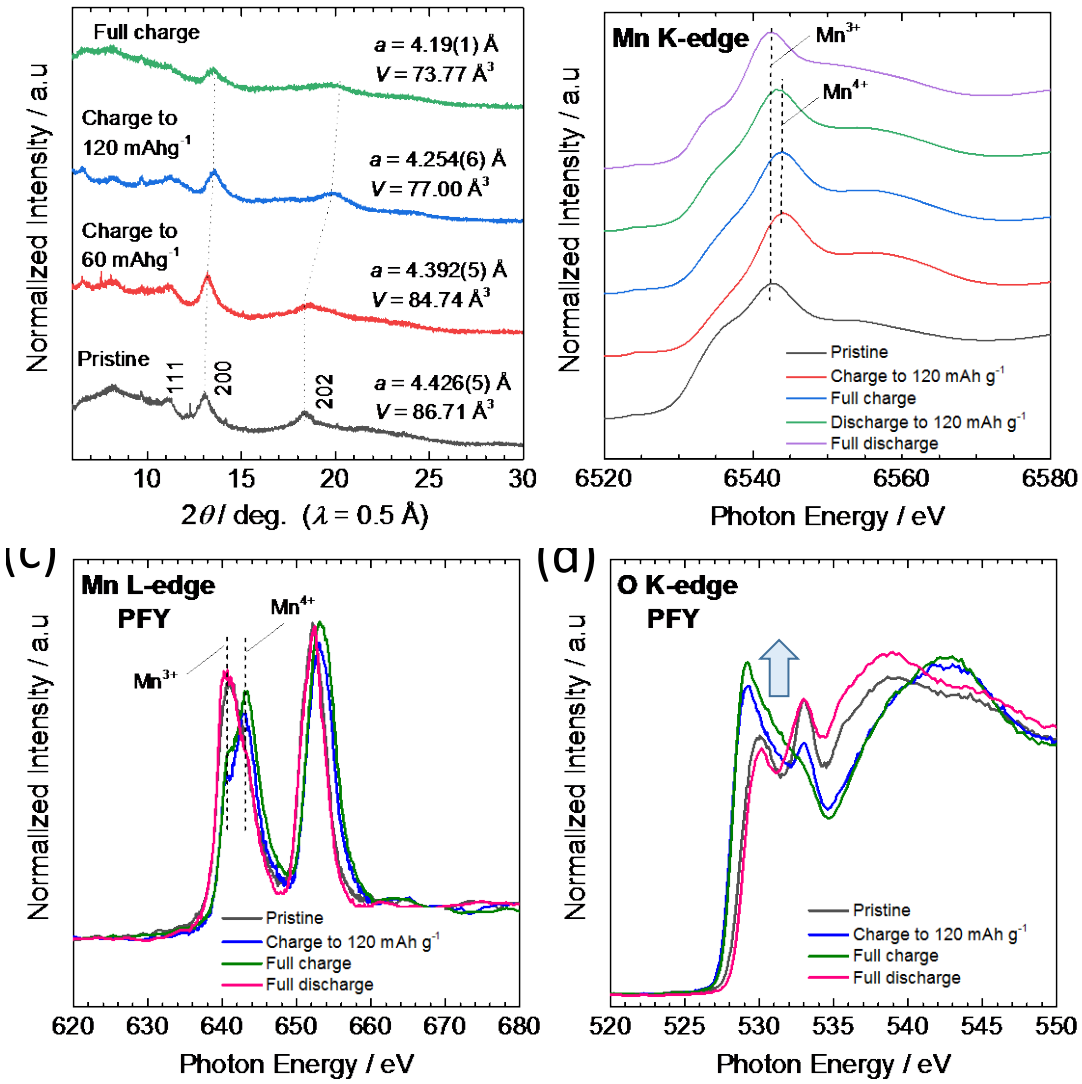

Figure 3. Reaction mechanisms of x $Na_2TiO_3 – (1 – x)$ $NaMnO_2$; (a) *ex-situ* synchrotron XRD patterns of $Na_{1.14-y}Mn_{0.57}Ti_{0.29}O_2$ on the initial charge process. XAS spectra of $Na_{1.14-y}Mn_{0.57}Ti_{0.29}O_2$ at (b) Mn K-edge, (c) Mn L-edge, and (d) O K-edge with different charge/discharge conditions. (Revised)

Figure 3b shows changes in Mn K-edge XAS spectra at different charge and discharge

states for $Na_{1.14-y}Mn_{0.57}Ti_{0.29}O_2$. On charge to 120 mA h g^{-1}, clear peak shift to a higher energy region is observed, indicating oxidation of trivalent Mn ions to higher oxidation state. Upon further charge to 4.5 V, clear changes in the peak position and profiles are not observed. A similar trend is also noted for Mn L-edge XAS spectra as shown in **Figure 3c**. Instead of oxidation of Mn ions, a clear change in O K-edge XAS spectra is noted at the plateau region in **Figure 3d**. Increase in the peak intensity at *ca*. 530 eV is often observed for Li-excess manganese-based oxides.[16, 35, 36] Recently, this peak has been proposed to originate from re-hybridization of O 2p and Mn e_g orbitals.[37] Holes in O 2p orbitals induced by electrochemical oxidation would be energetically stabilized by electron back donation from a Mn t_{2g} orbital. However, the appearance of this peak is more clearly pronounced for the Li system.[34] It is expected that much longer bond lengths for the Na-excess system with the rocksalt structure compared with the Li system simply result in weaker interaction between Mn t_{2g} and O 2p orbitals, possibly leading to less changes in O K-edge XAS spectra. Nevertheless, upon discharge, profiles of Mn L-edge and O K-edge XAS spectra are almost recovered to those of the as-prepared electrode, indicating that reversible redox reaction of oxide ions takes place. This trend is clearly different from that of the Nb system.[24] Oxygen loss was a dominative process for the Nb system on charge, and thus reduction of Mn ions, partly to Mn^{2+}, was observed on discharge. Mn reduction to Mn^{2+} is not observed for the Ti system, and the oxidation state of

Mn ions remains as a trivalent state on discharge. In addition, reduction of Ti ions is not found in the Ti L-edge XAS spectra after discharge as shown in **Supporting Figure S6**. From these results, it is concluded that reversibility of anionic redox reaction is highly improved for the Ti system even though higher Na contents result in small reversible capacities as electrode materials (**Figure 2a** and **b**). Note that $Na_{1.3}Mn_{0.4}Nb_{0.3}O_2$ and $Na_{1.2}Mn_{0.4}Ti_{0.4}O_2$ contain 40 mol% of Mn^{3+} ions in the structures, and similar electronic conductivity is, therefore, expected for both phases. However, the sodium content is higher (10 mol%) for the Nb system, possibly leading to higher reversible capacity associated with higher percolation probability and a lower Na migration barrier.[38]

In conclusion, it has been succeeded in synthesis of metastable Na-excess oxides with the cation-disordered rocksalt structure, which is found in the binary system of Na_2TiO_3–$NaMnO_2$, through the mechanical milling route. $Na_{1.14}Mn_{0.57}Ti_{0.29}O_2$ delivers a large reversible capacity on the basis of both cationic Mn^{3+}/Mn^{4+} and anionic O^{2-}/O^{n-} redox. Moreover, reversibility of anionic redox has been highly improved compared with the binary system with Na_3NbO_4. Anionic redox is an important strategy to design high-capacity and high-energy sodium insertion materials, and this finding possibly leads to the development of high-energy rechargeable Na batteries without less abundant elements, for instance, Li, Ni, and Co ions, in the future.

Acknowledgements

NY acknowledges the partial support from JSPS KAKENHI Grant Number 15H05701, 18H02076 and 19H05816, and MEXT program “Elements Strategy Initiative to Form Core Research Center”, MEXT; Ministry of Education Culture, Sports, Science and Technology, Japan. The synchrotron X-ray absorption work was done under the approval of the Photon Factory Program Advisory Committee (Proposal No. 2019G033). The experiment was performed (The XAS data were obtained) at SR center, Ritsumeikan University under the approval of Program Review Committee (S16010). The synchrotron radiation experiments were performed at the BL19B2 of SPring-8 with the approval of the Japan Synchrotron Radiation Research Institute (JASRI) (Proposal 2018B1811). TEM observation was supported by Dr Keisuke Shinoda, NIMS, Battery Research Platform with support by NIMS microstructural characterization platform as a program of "Nanotechnology Platform" of the Ministry of Education, Culture, Sports, Science and Technology (MEXT), Japan.

References

1. Slater, M. D.; Kim, D.; Lee, E.; Johnson, C. S., *Adv. Funct. Mater.* **2012,** *23*, 947-958. DOI 10.1002/adfm.201200691.

2. Kim, H.; Kim, H.; Ding, Z.; Lee, M. H.; Lim, K.; Yoon, G.; Kang, K., *Advanced Energy Materials* **2016,** *6*, 1-38. DOI 10.1002/aenm.201600943.

3. Barpanda, P.; Liu, G.; Ling, C. D.; Tamaru, M.; Avdeev, M.; Chung, S. C.; Yamada, Y.; Yamada, A., *Chemistry of Materials* **2013,** *25*, 3480-3487. DOI 10.1021/cm401657c.

4. Barpanda, P.; Nishimura, S. I.; Yamada, A., *Advanced Energy Materials* **2012,** *2*, 841-859. DOI

10.1002/aenm.201100772.

5. Barpanda, P.; Oyama, G.; Nishimura, S. I.; Chung, S. C.; Yamada, A., *Nature Communications* **2014,** *5*. DOI 10.1038/ncomms5358.

6. Lu, Z.; Dahn, J. R., *J. Electrochem. Soc.* **2001,** *148*, A1225. DOI 10.1149/1.1407247.

7. Mendiboure, A.; Delmas, C.; Hagenmuller, P., *Journal of Solid State Chemistry* **1985,** *57*, 323-331. DOI 10.1016/0022-4596(85)90194-X.

8. Yabuuchi, N.; Kajiyama, M.; Iwatate, J.; Nishikawa, H.; Hitomi, S.; Okuyama, R.; Usui, R.; Yamada, Y.; Komaba, S., *Nature Materials* **2012,** *11*, 512-517. DOI 10.1038/nmat3309.

9. Yoshida, H.; Yabuuchi, N.; Komaba, S., Na Insertion Mechanism in Alpha NaFeO2 as Positive Electrode Materials for Na-Ion Batteries. In *ECS Meet. Abstr. MA2012-02*, **2011**; Vol. 201, p 1850.

10. Zhao, J.; Zhao, L.; Dimov, N.; Okada, S.; Nishida, T., *J. Electrochem. Soc.* **2013,** *160*, A3077-A3081. DOI 10.1149/2.007305jes.

11. Yabuuchi, N.; Komaba, S., *Sci. Technol. Adv. Mater.* **2014,** *15* (4), 043501. DOI 10.1088/1468-6996/15/4/043501.

12. Zhao, W.; Tsuchiya, Y.; Yabuuchi, N., *Small Methods* **2019,** *3* (4), 1800032. DOI 10.1002/smtd.201800032.

13. Assat, G.; Delacourt, C.; Corte, D. A. D.; Tarascon, J.-M., *J. Electrochem. Soc.* **2016,** *163* (14), A2965-A2976. DOI 10.1149/2.0531614jes.

14. Lee, J.; Seo, D.-H.; Balasubramanian, M.; Twu, N.; Li, X.; Ceder, G., *Energy Environ. Sci.* **2015,** *8* (11), 3255-3265. DOI 10.1039/C5EE02329G.

15. Yabuuchi, N., *Chemistry Letters* **2017,** *46*, 412-422. DOI 10.1246/cl.161044.

16. Yabuuchi, N.; Nakayama, M.; Takeuchi, M.; Komaba, S.; Hashimoto, Y.; Mukai, T.; Shiiba, H.; Sato, K.; Kobayashi, Y.; Nakao, A.; Yonemura, M.; Yamanaka, K.; Mitsuhara, K.; Ohta, T., *Nature Communications* **2016,** *7*, 13814. DOI 10.1038/ncomms13814.

17. Yabuuchi, N.; Hara, R.; Kajiyama, M.; Kubota, K.; Ishigaki, T.; Hoshikawa, A.; Komaba, S., *Adv. Energy Mater.* **2014,** *4* (13), 1301453. DOI 10.1002/aenm.201301453.

18. Du, K.; Zhu, J.; Hu, G.; Gao, H.; Li, Y.; Goodenough, J. B., *Energy Environ. Sci.* **2016,** *9* (8), 2575-2577. DOI 10.1039/C6EE01367H.

19. Yabuuchi, N.; Hara, R.; Kubota, K.; Paulsen, J.; Kumakura, S.; Komaba, S., *J. Mater. Chem. A* **2014,** *2*, 16851-16855. DOI 10.1039/C4TA04351K.

20. Maitra, U.; House, R. A.; Somerville, J. W.; Tapia-Ruiz, N.; Lozano, J. G.; Guerrini, N.; Hao, R.; Luo, K.; Jin, L.; Pérez-Osorio, M. A.; Massel, F.; Pickup, D. M.; Ramos, S.; Lu, X.; McNally, D. E.; Chadwick, A. V.; Giustino, F.; Schmitt, T.; Duda, L. C.; Roberts, M. R.; Bruce, P. G., *Nature Chemistry* **2018**. DOI 10.1038/nchem.2923

21. Mortemard de Boisse, B.; Liu, G.; Ma, J.; Nishimura, S.-i.; Chung, S.-C.; Kiuchi, H.; Harada, Y.; Kikkawa, J.; Kobayashi, Y.; Okubo, M.; Yamada, A., *Nature Communications* **2016,** *7*, 11397. DOI

10.1038/ncomms11397.

22. Rozier, P.; Sathiya, M.; Paulraj, A.-R.; Foix, D.; Desaunay, T.; Taberna, P.-L.; Simon, P.; Tarascon, J.-M., *Electrochem. Commun.* **2015,** *53*, 29-32. DOI 10.1016/j.elecom.2015.02.001.

23. Perez, A. J.; Batuk, D.; Saubanère, M.; Rousse, G.; Foix, D.; McCalla, E.; Berg, E. J.; Dugas, R.; H. W. van den Bos, K.; Doublet, M.-L.; Gonbeau, D.; Abakumov, A. M.; Van Tendeloo, G.; Tarascon, J.-M., *Chem. Mater.* **2016,** *28* (22), 8278-8288. DOI 10.1021/acs.chemmater.6b03338.

24. Sato, K.; Nakayama, M.; Glushenkov, A. M.; Mukai, T.; Hashimoto, Y.; Yamanaka, K.; Yoshimura, M.; Ohta, T.; Yabuuchi, N., *Chem. Mater.* **2017,** *29* (12), 5043-5047. DOI 10.1021/acs.chemmater.7b00172.

25. Izumi, F.; Momma, K., *Solid State Phenom.* **2007,** *130*, 15-20.

26. Momma, K.; Izumi, F., *J. Appl. Crystallogr.* **2011,** *44* (6), 1272-1276. DOI doi:10.1107/S0021889811038970.

27. Meng, F.; Liu, Y.; Xue, T.; Su, Q.; Wang, W.; Qi, T., *RSC Advances* **2016,** *6* (113), 112625-112633. DOI 10.1039/C6RA16984H.

28. Kitajou, A.; Kobayashi, E.; Okada, S., *Electrochemistry* **2015,** *83* (10), 885-888. DOI 10.5796/electrochemistry.83.885.

29. Hoshino, S.; Glushenkov, A. M.; Ichikawa, S.; Ozaki, T.; Inamasu, T.; Yabuuchi, N., *ACS Energy Letters* **2017,** *2* (4), 733-738. DOI 10.1021/acsenergylett.7b00037.

30. Sato, T.; Sato, K.; Zhao, W.; Kajiya, Y.; Yabuuchi, N., *Journal of Materials Chemistry A* **2018,** *6* (28), 13943-13951. DOI 10.1039/C8TA03667E.

31. Sakuda, A.; Kuratani, K.; Takeuchi, T.; Kiuchi, H.; Kawaguchi, T.; Shikano, M.; Sakaebe, H.; Kobayashi, H., *Electrochemistry* **2017,** *85* (9), 580-584. DOI 10.5796/electrochemistry.85.580.

32. Pan, M.; Hakari, T.; Sakuda, A.; Hayashi, A.; Suginaka, Y.; Mori, S.; Tatsumisago, M., *Electrochemistry* **2018,** *86* (4), 175-178. DOI 10.5796/electrochemistry.17-00104.

33. Shi, T.; Xiao, P.; Kwon, D.-H.; Sai Gautam, G.; Chakarawet, K.; Kim, H.; Bo, S.-H.; Ceder, G., *Chem. Mater.* **2018,** *30* (24), 8811-8821. DOI 10.1021/acs.chemmater.8b03490.

34. Yabuuchi, N., *The Chemical Record* **2019,** *19* (4), 690-707. DOI 10.1002/tcr.201800089.

35. Oishi, M.; Yamanaka, K.; Watanabe, I.; Shimoda, K.; Matsunaga, T.; Arai, H.; Ukyo, Y.; Uchimoto, Y.; Ogumi, Z.; Ohta, T., *Journal of Materials Chemistry A* **2016,** *4* (23), 9293-9302. DOI 10.1039/C6TA00174B.

36. Luo, K.; Roberts, M. R.; Hao, R.; Guerrini, N.; Pickup, D. M.; Liu, Y.-S.; Edström, K.; Guo, J.; Chadwick, A. V.; Duda, L. C.; Bruce, P. G., *Nature Chemistry* **2016,** *8* (7), 684-691. DOI 10.1038/nchem.2471

37. Okubo, M.; Yamada, A., *ACS Appl. Mater. Interfaces* **2017,** *9* (42), 36463-36472. DOI 10.1021/acsami.7b09835.

38. Urban, A.; Lee, J.; Ceder, G., *Adv. Energy Mater.* **2014,** *4* (13), 1400478-n/a. DOI

10.1002/aenm.201400478.

TOC